Optimization of an HT-PEM fuel cell based residential micro combined heat and power system: A multi-objective approach

Alireza Haghighat Mamaghani, Behzad Najafi*, Andrea Casalegno, Fabio Rinaldi

Dipartimento di Energia, Politecnico di Milano, Via Lambruschini 4, 20156, Milano, Italy

This article presents multi-objective optimization of an HT-PEM fuel cell based micro CHP system under steady-state operation by employing the mathematical model of the plant previously developed by our group. Different optimization procedures have been carried out to find the optimal points while considering two sets of objective functions: I) thermal power generation and net electrical output and II) net electrical efficiency and thermal efficiency. In the first part of the work, optimization has been performed at full load operation with electrical and thermal generation as objectives. The obtained Pareto frontier shows the capability of the system to cater a broad range of electrical demand (21.0 kW-29.4 kW) while offering the maximum achievable thermal generation. In the next step, in order to find the optimal operating conditions of the system while addressing specific thermal and electrical load profiles, a series of Pareto fronts have been acquired at different fuel partialization levels. Finally, using the primary energy saving (PES) index, the best operating points, in terms of electrical and thermal efficiency, have been determined. It was observed that the net electrical efficiency up to 32.3% and thermal efficiency as high as 61.1% can be reached through the optimization.

Keywords: Combined heat and power, High temperature, PEM fuel cell, Genetic algorithm,Multi objective optimization, Primary energy saving

1. Introduction

Due to the concerns regarding the global warming and more stringent environmental regulations (Lau et al., 2012), specifically in Europe, there is an increasing pressure on power generation technologies to operate in a more cost-effective (Tran and Smith, 2017), efficient, and environment-friendly manner (Zhai et al., 2014). Buildings are determined to account for around 40% the total energy consumptions and 36% of GHG emissions in Europe. Residential buildings constitute about 75% of the total European building floor area, where a significant share (up to 80%) of their energy use is related to heating applications (Merkel et al., 2017). Furthermore, decentralized generation (DG) has been found to be a promising alternative for decreasing the carbon intensity of the energy supply (Bazmi et al., 2015) by evading the transmission and distributions losses (Fuchs and Hinderer, 2016). The latter approach can also lead to an improvement in the energy efficiency as the waste heat can be utilized to cater the heating demand (Merkel et al., 2017). Micro-CHP systems based on highly efficient and environmentally-friendly power generation technologies, which can address both the electrical and the thermal demands of residential buildings, have received increasing attentions in the recent years (Elmer et al., 2015).

Fuel cells are recognized as one of the most promising electricity generation technologies (Stambouli, 2011), both for stationary (Pirkandi et al., 2017) and automotive applications (Rizzi et al., 2014). The advantages of fuel cell units include elevated energy efficiency (Sharaf and Orhan, 2014), cleaner operation (Wee, 2010), lower noise, higher reliability, and the ability to produce electricity and heat simultaneously (Pirkandi et al., 2012). In the transportation sector, fuel cell technology has received interest as a propulsion alternative for various means of transport including passenger vehicles (Evangelisti et al., 2017), recreational vehicles (Benveniste et al., 2017) and buses (Hua et al., 2014). As stationary power generation systems, fuel cell based micro-combined heat and power units have been found to be favorable options to efficiently meet the heating and the electricity demands of residential dwellings (Mehrpooya et al., 2017).

Among different fuel cell technologies, proton exchange membrane fuel cell (PEM FC) is the most widely utilized technology (Wee, 2007) thanks to its advantageous features such as low

Article history:
Received 4 June 2017
Received in revised form 16 January 2018
Accepted 17 January 2018
Available online 19 January 2018

* Corresponding author.
E-mail addresses: alireza.haghighat@mail.polimi.it (A. Haghighat Mamaghani), behzad.najafi@polimi.it (B. Najafi), andrea.casalegno@polimi.it (A. Casalegno), fabio.rinaldi@polimi.it (F. Rinaldi).

Published Journal Article available at https://doi.org/10.1016/j.jclepro.2018.01.124

Nomenclature

Acronyms

aux/proc	auxiliary to process flow rate ratio
CHP	combined heat and power
GDL	gas diffusion layer
HT-PEM	high temperature proton exchange membrane
LMTD	logarithmic mean temperature difference
LT-PEM	low temperature proton exchange membrane
MEA	membrane electrode assembly
OHM	ohmic
PBI	polybenzimidazole
PES	primary energy saving
PFSA	perfluorosulfonic acid
RF	reforming factor
S/C	steam to carbon ratio
SMR	steam methane reforming
WGS	water gas shift
WKO	water knock out

Symbols

E_{ID}	ideal voltage (V)
E_a	activation energy (kJ mol^{-1})
f	friction factor
ΔH_{298K}	standard enthalpy of reaction (kJ kmol^{-1})
I	current (A)
k	rate coefficient
K	equilibrium constant
LHV	low heating value (kJ kg^{-1})
$\dot{m}$	mass flow rate (kg s^{-1})
N	number of cells
Nu	Nusselt number
P_x	partial pressure of species x
P	power (kW)
Pr	Prandtl number
$\dot{Q}$	the time rate of heat transfer (kW)
r	rate of reaction (mol lit^{-1} s^{-1})
R	universal gas constant (kJ kmol^{-1} K^{-1})
Re	Reynolds number
T	temperature (K)
V	voltage (V)

Subscripts

A	anode
B	burner
C	cathode
cogen	cogeneration
el	electrical
th	thermal

Greek symbols

η_A	anodic voltage loss
η_C	cathodic voltage loss
η_{el}	electrical efficiency
η_I	first law efficiency
η_{th}	thermal efficiency
λ_{H_2}	anodic stoichiometric ratio

operating temperature, high power density (Wang et al., 2011), quick response to load changes (Chatrattanawet et al., 2017), and compactness (Basu, 2015). PEM FC based units are the most broadly employed fuel cell based residential technology (Elmer et al., 2015). The most commercially established PEM fuel cell technology is the conventional low temperature PEM fuel cell (LT-PEM FC) (Gandiglio et al., 2014). Several studies have been focused on of LT-PEM FC based CHP system, including studies focused on performance investigation (Ham et al., 2015), parametric study (Kang et al., 2015), and reliability investigation (Wang, 2017) of these units. Other studies have also been dedicated to techno-economic analysis (Hawkes et al., 2009; Napoli et al., 2015), and optimization (Godat and Marechal, 2003; Hubert et al., 2006) of these systems. Nevertheless, LT-PEM FC technology suffers from several operational issues including water management problems, low CO tolerance, and necessity of intensive cooling. Therefore, high temperature PEM FC has attracted a great deal of attention owing to its capability of overcoming the mentioned drawbacks associated with the LT-PEM FCs (Arsalis et al., 2013).

Several research activities have been carried out on investigating the application of HT-PEM fuel cells for cogeneration and micro-CHP purposes. Colella and Pilli (Colella and Pilli, 2015) performed an energetic and thermo-economic analysis on the HT-PEM fuel cell based CHP systems in light commercial buildings. They showed that the average per-unit cost (PUC) of electrical power is estimated to span 15–19,000 kWe and the average PUC of electrical and heat recovery power is 7000–9000 kW. In another work, Dillon and Colella (Dillon and Colella, 2015) analysed the measured performance data from 5kWe HT-PEM fuel cell based CHP systems. They observed that the net electric efficiency averages 33.7% (based on HHV) which is slightly below the manufacturer's stated rated electric efficiency of 36%. Herdem et al (Herdem et al., 2015). conducted a modelling and parametric study on a methanol reformate gas fuelled HT-PEM FC based system. Their results revealed that the effect of CO molar ratio on the fuel cell performance decreases at elevated fuel cell temperatures. The fuel cell voltage decreases almost 78% with the variation of the current density from 0.1 A/cm^2 to 1 A/cm^2 for 160 °C fuel cell temperature and 0.9% CO molar ratio in the reformate gas. Cappa et al (Cappa et al., 2015). compared the technical and economical performances of an HT-PEMFC based CHP unit with those of an internal combustion engine for a 10 kW residential CHP application. They demonstrated that the internal combustion engine is much more affected by the choice of operating strategy with respect to the fuel cell, in terms of long-term profitability.

Some previous studies have also been devoted to the optimization of HT-PEM fuel cell based micro-CHP units, most of which considered only one objective in the optimization procedure. Arsalis et al (Arsalis et al., 2013). carried out a study focused on optimization of 1 kW_{el} micro-CHP system based on HT-PEMFC technology which caters the demand of a single family household. In another study (Arsalis et al., 2015), Arsalis et al. optimized the operating conditions of a residential HT-PEM FC based micro-CHP system coupled with a vapor-compression heat pump. Their results demonstrated an average net electrical efficiency of 0.380 and an average total system efficiency of 0.815.

The present paper is focused on optimizing the operating condition of an HT-PEM fuel cell based micro-CHP plant for a wide range of electrical and thermal generation levels, in order to maximise the performance of the unit while addressing the

intermitted demand of a residential building. A detailed mathematical model of the plant, developed in a previous study conducted by the authors (Najafi et al., 2015a), has been utilized in this work with some minor modifications to facilitate the optimization procedure. In the abovementioned study, the authors performed a sensitivity analysis on the key parameters of the fuel processor (steam to carbon ratio and the auxiliary to process flow rate) and the fuel cell stack (cell operating temperature, current density and the anodic stoichiometric ratio) to evaluate the system's performance under different operating conditions. In another work (Najafi et al., 2015b), the authors applied fuel partialization (i.e. changing fuel input) and power to heat shifting (i.e. altering the anodic stoichiometric ratio) strategies on the same plant to investigate the capability of the system to deal with intermittent electrical and thermal load profiles. The present study is a continuation of our previous works with the intention of exploiting the heretofore gained understanding and proposing an optimization approach to find the optimal operating parameters while providing broad ranges of electrical and thermal generations. Based on our previous studies (Najafi et al., 2015a, 2015b), steam to carbon ratio, auxiliary to process fuel ratio, anodic stoichiometric ratio, and burner outlet temperature are considered as optimization parameters. Furthermore, the allowed ranges of variations of each operating condition in the optimization procedure, are chosen based on the results of the first study and the corresponding practical constraints.

Two different optimization procedures have been carried out at full load and partial load operation conditions: i) optimization procedure I with net electrical power and thermal power as objectives and ii) optimization procedure II in which the considered objectives are the net electrical efficiency and thermal efficiency. The results of the optimization procedures are a series of optimal operating points (Pareto fronts) at full/partial loads, which enable addressing intermittent electrical/thermal loads while achieving the maximum possible performance indices. In the last section of the research, considering the primary energy saving index, the best optimal point is selected among the Pareto front solutions and the corresponding electrical and thermal generation along with the resulting efficiencies are reported.

It is noteworthy that the main contribution of the present study, compared to the previous works of the authors on this subject, including (Haghighat Mamaghani et al., 2017), is to provide multiple optimal operating conditions with various electrical and thermal generation levels. Utilizing the proposed set of optimal operating points can guarantee the maximization of system's performance while supplying intermittent residential demand profiles.

2. Plant description

Fig. 1 shows the configuration of the HT-PEM fuel cell based CHP plant, which is fed by natural gas. The fuel is firstly divided into two streams; the first of which is going through the desulfurization process and is later introduced into the ejector and the second one is injected to the burner. In the ejector, the fuel is mixed with the superheated water (node 24) coming out of the superheater. The mixture of natural gas and superheated steam is then fed to the SMR reactor, where the natural gas is converted to a hydrogen rich reformate gas via reforming reactions. The steam methane reforming reactions are endothermic (except WGS) and the required heat is provided by the combustion gases from the burner. Since the temperature of the combustion gases leaving SMR reactor is still high, the available energy of this stream (node 15) is firstly used to produce the required superheated steam for the SMR reactions and afterwards to warm up the water in the economizer. Although HT-PEMFC CO tolerance is higher than LT-PEMFC one, the amount of CO in the syngas (node 7) is much higher than the tolerable level of CO content for the anodic side of the fuel cell stack. As a result, a WGS reactor is placed after the SMR reactor, which not only decreases the amount of CO via water gas shift reaction but also increases the H_2 selectivity. The heat exchanger prior to the WGS reactor cools the syngas (node 7) down to about 300 °C while preheating the water before entering the superheater. The WGS outlet stream (node 9) passes through the anodic recuperator, a heat exchanger and finally water knock out (WKO) before being injected into the anodic side of the HT-PEM stack (node 13). In the air side, the compressed air (node 34) is fed to the cathodic side of the fuel cell stack after its temperature is increased via cathodic recuperator. In the fuel cell stack, hydrogen is consumed via the electrochemical reaction producing electricity, water and heat. The outlet stream of the anodic side (node 14) is introduced into the burner where the unreacted methane and hydrogen is burned with the auxiliary natural gas and air to provide the required heat in the SMR reactor. In order to reach the desired temperature at the outlet of the burner (node 6), a separate air stream has been considered to be injected into the burner. It is worth mentioning that the stack is cooled down by an oil circulation unit, which later releases the absorbed heat to the Thermal user 1. In order to provide the reader with a better understanding of the operation principle of the plant, the temperature, molar flow rate and composition of the important nodes in Fig. 1, under an operating conditions extracted from our previous study (Najafi et al., 2015a) ($S/C = 5.25$, $aux/proc = 0.18$, $T_B = 1193$, and $\lambda_{H_2} = 1.2$), are given in Table 1.

3. Mathematical model of components

In the present section, assumptions and modelling methodologies, which are employed in order to simulate the key components of the plant, are provided.

3.1. Steam methane reformer

The kinetic model put forward by Xu and Froment (Xu and Froment, 1989) for steam methane reforming has been employed in the modeling process of SMR. A one dimensional steady state and non-isothermal plug flow reactor with shell and tube heat exchanger design has been developed in the MATLAB environment and the obtained data from simulation have been validated with the experimental data provided by our industrial partner. In the SMR model, two separate media have been taken into account: (i) tube side or catalytic bed where the reactions happen and (ii) shell side where the hot gas from burner supplies heat for endothermic reactions. Based on the Xu and Froment (Xu and Froment, 1989) kinetic model, water–gas shift reaction was considered to take place in parallel with the steam reforming reactions.

The three key reactions occur in a steam reformer can be listed as:

$$CH_4 + H_2O \Leftrightarrow CO + 3H_2 \qquad \Delta H_{298K} = +206\ kJ/mol \tag{1}$$

$$CO + H_2O \Leftrightarrow CO_2 + H_2 \qquad \Delta H_{298K} = -41\ kJ/mol \tag{2}$$

$$CH_4 + 2H_2O \Leftrightarrow CO_2 + 4H_2 \qquad \Delta H_{298K} = +165\ kJ/mol \tag{3}$$

The details of the kinetics of the reforming reactions, kinetic

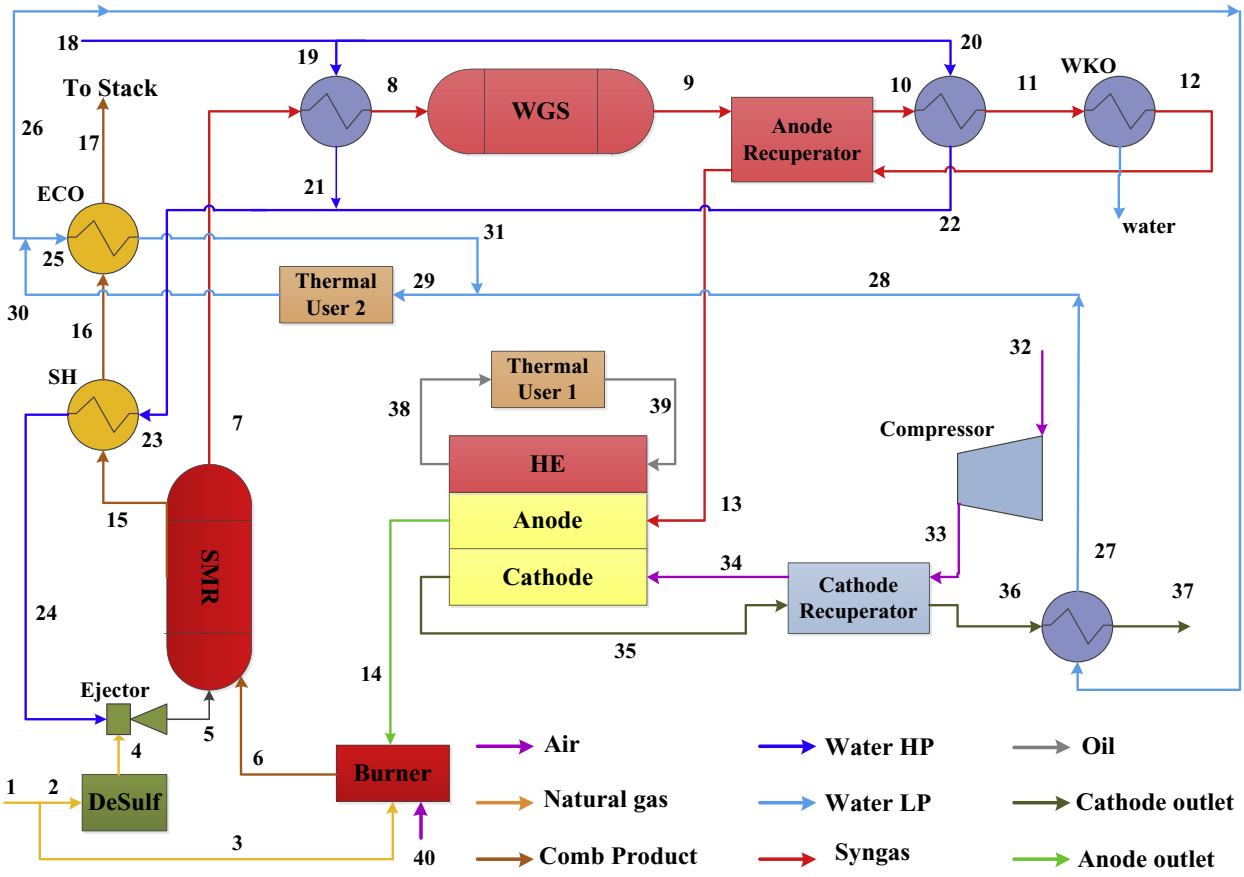

Fig. 1. Schematic view of the HT-PEMFC based plant.

Table 1
Properties of the main nodes of the CHP system under design operating variables.

Node	Temperature (°C)	Flow rate (mol/s)	Composition (mole fraction)						
			H_2O	CH_4	H_2	CO	CO_2	N_2	O_2
5	414	0.666	84.01	15.73	0.00	0.00	0.00	0.26	0.00
6	920	1.639	13.11	0.00	0.00	0.16	7.39	68.17	11.17
7	567	0.828	49.77	2.86	37.37	1.81	7.98	0.21	0.00
8	320	0.828	49.77	2.86	37.37	1.81	7.98	0.21	0.00
9	338	0.829	48.27	2.86	38.87	0.33	9.47	0.21	0.00
13	130	0.554	22.68	4.28	58.09	0.49	14.16	0.31	0.00
14	160	0.234	31.89	10.32	23.24	1.11	33.43	0.00	0.00
15	609	1.639	13.11	0.00	0.00	0.16	7.39	68.17	11.17
34	90	1.284	0.00	0.00	0.00	0.00	0.00	79.10	20.90
35	160	1.468	21.66	0.00	0.00	0.00	0.00	69.17	9.17

coefficients, and the assumptions can be found in the literature (Xu and Froment, 1989).

3.2. High temperature PEM fuel cell stack

The HT-PEM fuel cell stack is made up of three main parts including the membrane electrode assembly (MEA), pre-heater, and oil cooling circuit. In the first section, pre-heater, the reactants (syngas and compressed air) exchange heat with the circulating oil to reach the desired temperature. In the MEA, hydrogen and oxygen go through oxidation and reduction reactions and eventually produce water and electricity. The MEA has three main parts: cathode and anode channels, the gas diffusion layer (GDL) as a pathway for reactants to reach the catalyst layer, and the anodic and cathodic electrodes where the electrochemical reaction occurs. The MEA domain is modelled using a quasi 2D approach: one coordinate of integration is along the channel and the other one is along the thickness of the MEA. Within the channel, the hydrogen and oxygen are gradually consumed owing to the electrochemical reactions and, as a result, water is produced. Mass conservation is taken into account to determine the species concentration profiles along the channels, especially oxygen, hydrogen, water and carbon monoxide. The main geometric parameters of the fuel cell stack can be found in a previous study conducted by the authors (Haghighat Mamaghani et al., 2015).

The reaction rate (the current density) is calculated using the following equation, which relates the cell voltage to the ideal voltage:

$$V = E_{ID} - \eta_{OHM} - \eta_C - \eta_A \tag{4}$$

$$P_{stack} = V_{cell} I_{stack} N \tag{5}$$

where V is the single cell voltage, E_{ID} is the ideal voltage by Nernst equation, η_{OHM} is the ohmic loss, and η_C and η_A are the cathode and anode activation losses.

The Ohmic loss is assessed from Ohm's law and is the summation of the resistances of the GDLs, bipolar plate, and the electrolyte. It is presumed that the electrolyte conductivity follows Arrhenius law and it is taken from (Siegel et al., 2011). The Ohmic losses of the electrolyte are calculated using the proton conductivity of the electrolyte:

$$\eta_{ohm} = \frac{i\,\delta_m}{\sigma_{PBI/H_3PO_4}\ (T)} \tag{6}$$

where

$$\sigma_{PBI/H_3PO_4}\ (T) = \frac{\sigma}{T} exp\left(-\frac{E_a}{RT}\right) \tag{7}$$

Mass transport within the GDL is modelled based on the multi component gas diffusion using Stefan-Maxwell phenomenological law (Pisani, 2008). The cathodic electrode is considered to be homogeneous and its activation losses are supposed to follow the Tafel Law, first order with respect to oxygen concentration (Liu et al., 2006):

$$\eta_C \equiv b \cdot \log\left(\frac{i}{i_*}\right) + b \cdot \log\ \left(\frac{C_{ref}}{C_{O_2,el}}\right) \tag{8}$$

where i_* is the reference exchange current density which follows an Arrhenius like behavior and b which is calculated using the following relation, is the Tafel slope:

$$b = RT/(\alpha_C F) \tag{9}$$

The adverse effect of catalyst CO poisoning on the cell voltage and the performance of the fuel cell has been also incorporated in the formulation of anodic activation losses. The hydrogen and CO oxidation currents are computed by means of the Butler-Volmer equation (Baschuk and Li, 2003).

$$i_{H2} \equiv i_{*,H2} \cdot \vartheta_H \cdot 2\ \sinh\left(\frac{\eta_A}{b_A}\right) \tag{10}$$

$$i_{CO} \equiv i_{*,CO} \cdot \vartheta_{CO} \cdot 2\ \sinh\left(\frac{\eta_A}{b_A}\right) \tag{11}$$

$$i = i_{CO} + i_{H_2} \tag{12}$$

where, by definition, the sum of the coverage of all the species must be equal to 1:

$$\vartheta_{FREE} = 1 - \vartheta_H - \vartheta_{CO} - \vartheta_{H_2PO_4^-} \tag{13}$$

The coverage of phosphoric acid ($\vartheta_{H_2PO_4-}$) is taken from (Bergmann et al., 2010) while the coverage of hydrogen and CO (ϑ_H and ϑ_{CO}) are calculated considering the equilibrium of adsorption using Langmuir adsorption for hydrogen and Frumkin adsorption for carbon monoxide. The values of the parameters, employed in the HT-PEM fuel cell stack model, are given in the previous work of the authors (Najafi et al., 2015a).

It is worth pointing out that HT-PEM fuel cell units suffer from degradation, which decreases their performance in the long-run. The decline in the performance depends on the characteristics of the materials employed in the cathode, the anode and the membrane. However, the scope of the present work is to conduct a general optimization of operating conditions of the system, at various thermal and electrical generation levels, in the beginning of operation. Therefore, in the present study, the steady state operation of the system is only modelled and the degradation phenomenon has been neglected.

3.3. Ejector

In order to model the ejector, a single phase thermodynamic model, presented by Eames et al(Eames et al., 1995). based on isobaric mixing (He and Wang, 2009), has been employed. As demonstrated in Fig. 2, the ejector is considered to be made up of four main sections including the nozzle, the suction chamber, the constant area, and the diffuser. In the developed model, the steam is taken into account as the primary fluid and the methane as the secondary one. The losses due to friction are introduced through considering isentropic efficiencies for the nozzle, the diffuser and the mixing chamber. The two fluids are also assumed to be mixed at the outlet of the nozzle and complete mixing is considered to takes place in the mixing chamber before the shock wave and in the constant area. Moreover, the gases are considered to be ideal and the flow to be one dimensional.

For the nozzle section the energy conservation equation is expressed as:

$$\frac{u_1^2}{2} = \eta_{nozzle}\ (h_{in} - h_1) \tag{14}$$

where the index 1 refers to the outlet section of the nozzle. For the mixing part, the momentum conservation equation between this section and the complete mixing section (m) is solved:

$$\eta_{mixing}\ (m_p\ u_{p1} - m_s\ u_{s1}) = (m_p + m_s)\ u_m \tag{15}$$

where the indexes p and s refer to the primary and secondary fluids. In this section using a correlation based on the Mach numbers before and after the wave, the pressure change due to the shock wave is also considered. In the last section, using the Mach number, the output pressure is evaluated as follows:

$$\frac{P_4}{P_3} = \left(\frac{(\gamma - 1)\ \eta_{diff}}{2}\ M_3^2 + 1\right)^{\frac{\gamma-1}{\gamma}} \tag{16}$$

Based on the values suggested by (Eames et al., 1995), the efficiencies of the three sections are assumed to be 0.85, 0.85, and 0.95. Starting from a guess outlet pressure, the outlet pressure of the primary nozzle is determined and, by solving the previously mentioned equations, the outlet conditions of the ejector will be calculated.

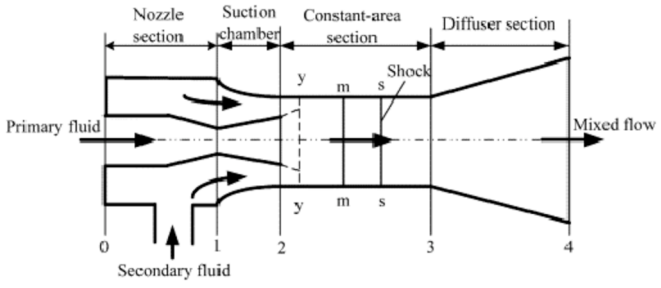

Fig. 2. The schematic of the ejector proposed by Eames et al(Eames et al., 1995). presented in (He and Wang, 2009).

It is worth mentioning that the applied efficiencies for different parts of the ejector might change while operating at various operating conditions (Liu and Groll, 2013; Varga et al., 2009). Determining such variations requires a more detailed ejector modelling methodology such as a CFD based approach (Besagni et al., 2015, 2017), which is beyond the scope of this study. Nevertheless, the variations in the mentioned efficiencies are considered to be within ±10% of the corresponding average values (Zheng and Deng, 2017) and the resulting effect on the overall electrical efficiency of the plant does not exceed 0.1%. As a result, the mentioned choice in the ejector modelling methodology does not affect the final results of the present work.

4. Plant simulation methodology and solving procedure

Considering the interdependence between the parameters of the plant, in order to obtain the thermodynamic properties at different nodes and the resulting performance indices at each operating condition, an iterative procedure should be implemented. The parameters which are considered in the main iterative procedure include the temperature of superheated water (node 24) and anode outlet molar flow rate for each compound (node 14). First, a guess value is considered for these two parameters and the simulation of the plant is carried out. After the simulation of the entire plant is completed, new values for these two parameters are determined and the guessed values are replaced with the average of their previous values and the determined ones. The mentioned iterative procedure is continued until the considered convergence criteria are met. The mentioned criteria necessitate that the difference between the values obtained for these parameters in the last two iterations would be less than 1%.

Regarding the simulation procedure at each iteration, for modelling the operation of the burner, since T_B (node 6) and amount of injected natural gas (node 3) are known, the molar flow rate of air stream is varied until the desired T_B is achieved. The latter procedure simulates a burner with a control system that keeps the stoichiometric ratio constant. As mentioned earlier, the desired temperature of syngas entering WGS reactor (node 8) is around 300 °C. The mass flow rate of water to pre-WGS heat exchanger (node 19) is iteratively varied until the desired temperature for node 8 is reached. Regarding the stack calculations, taking into consideration the stack design (our previous work) and the molar flow rate of hydrogen in stream 13, stack's current is determined and, in turn, the corresponding required amount of oxygen (i.e. air (node 32)). Finally, the molar flow rate of the anodic outlet (node 14) is obtained and its guess value is updated using the above-mentioned iterative procedure.

5. System optimization

5.1. Definition of objective functions

In the present study, while operating at full load condition, two different optimization procedures have been carried out. In the first procedure (Optimization procedure I), the generated net electrical power and the thermal power are considered as the objective functions. In the second procedure (Optimization procedure II), the net electrical efficiency and the thermal efficiency, which should be maximized, are the objective functions. It is noteworthy that even though the process fuel flow rate fed to the plant is kept constant, the auxiliary to process fuel flow rate ratio is one of the optimization parameters and the overall fuel flow rate fed to the plant is varying at different operating points. The results of the first and second optimization procedure are different and each of the corresponding results can be chosen and utilized considering the design criteria of a specific plant. In the second part of study, the second optimization procedure (considering efficiencies as objectives) is applied while operating at different partialization levels.

The net electrical efficiency considered in the second optimization procedure is defined as follows:

$$\eta_{net,el} = \frac{\dot{P}_{el,net}}{\dot{m}_{CH_4,in} LHV_{CH_4}} \tag{17}$$

where the net power output is the remaining power generated by the fuel cell stack after losses and subtracting auxiliaries. The thermal efficiency is similarly defined as:

$$\eta_{th} = \frac{\dot{Q}_{user1} + \dot{Q}_{user2}}{\dot{m}_{CH_4,in} LHV_{CH_4}} \tag{18}$$

It should be added that exergetic and economic objectives are other possible alternatives to be considered as objective functions in the optimization procedure. However, in the present study, the size of the system and the configuration of plant are kept constant, and the corresponding operating conditions are only optimized. Hence, utilizing these objectives does not lead to results, which are different from the ones obtained using energetic efficiency and their use is beyond the scope of this work.

5.2. Design parameters and constraints

Steam to carbon ratio (S/C), anodic stoichiometric ratio (λ_{H_2}), burner outlet temperature (TB) and fuel auxiliary to process ratio (aux/proc) have been chosen as design parameters. Considering the results of the sensitivity analysis that the authors had conducted in their previous study and taking into account the corresponding practical constraints, the range of variation of optimization parameters are considered to be:

$$3.5 < S/C < 5.5 \tag{19}$$

$$1.2 < \lambda H_2 < 2 \tag{20}$$

$$827 < T_B < 1027\ ^\circ C \tag{21}$$

$$0.12 < aux/proc < 0.22 \tag{22}$$

Due to exothermic nature of water gas shift reaction, the inlet temperature of the flow entering the WGS should be decreased according to the operating range of the corresponding reaction. The following constraint regarding the inlet temperature of WGS reactor is considered:

$$T_8 < 337\ ^\circ C \tag{23}$$

To avoid formation of carbonic acid (H_2CO_3), the temperature exhaust gases should not be lower than a certain level. The following constraint imposes the minimum allowable chimney temperature:

$$T_{17} > 67\ ^\circ C \tag{24}$$

More details regarding the operating conditions of the CHP plant are given in Table 2.

In LT-PEM FC plants, the cathodic flow should be extensively humidified and a humidifier should be integrated with the cathodic side of the stack. The humidifier in LT-PEM FC based plants results in a notable pressure drop, which makes the power consumption of the cathodic compressor considerable. However, in the case of HT-

Table 2
The fixed design parameters of the HT-PEMFC based CHP plant.

Operating condition	Value
Ambient temperature	20 (°C)
Ambient pressure	1 (10^5 Pa)
Pressure of high pressure water circuit	7.8 (10^5 Pa)
Pressure of low pressure water circuit (bar)	2 (10^5 Pa)
Cathodic stoichiometric ratio	2
Current density	0.2 ($A.cm^{-2}$)
Cell temperature	160 (°C)
Air compressor isentropic efficiency	82 (%)

PEM FC based units, cathodic humidification and thus the integrated humidifier is not needed. Given that, the consumption of cathodic compressor for these plants is not notable and the considered compressor efficiency does not play a significant role in the obtained overall performance of the plant.

5.3. Optimization method

In many engineering problems, there are different objectives, sometimes conflicting, which should be satisfied simultaneously. Unlike single-objective optimization problems, the result of a multi-objective optimization problem is not a unique optimal solution. The trade-off between the objectives leads to a set of non-dominated solutions, called the Pareto front, which satisfy the objective functions at an acceptable level without being dominated by others. The advantage of multi-objective optimization is the capability to optimize the system considering several conflicting objectives simultaneously while taking into account a number of equalities and inequalities. After obtaining the Pareto optimal solutions, the decision-maker can chose the best design vector based on the specific considered project. There are different methods to perform multi-objective optimization and achieve the Pareto front solutions. One of the most extensively used methods is the genetic algorithm which imitates the laws of natural evolution to find an optimal solution for a given optimization problem. The multi-objective GA implemented in MATLAB optimization toolbox has been employed in the present work and the chosen values for the GA parameters are listed in Table 3. In genetic algorithm, a solution vector is called a chromosome or an individual and is made of discrete units called genes. A solution vector is used to find the objective functions values (fitness value) and then new generations of solutions are produced from the previous ones employing crossover and mutation. In the crossover operation, two chromosomes (parents) are combined together to form new chromosomes (offsprings). Individuals with higher fitness have more chance for being chosen and generating offsprings. In the mutation operator, random changes into the properties of chromosomes are applied to help the population search to escape from local optima by introducing diversity into the population (Najafi et al., 2011). The flowchart in Fig. 3 demonstrates the overall procedure and various steps of GA optimization. The population size and number of generations are chosen through try and error considering the trade-off between the error (with respect to the global optima) and the calculation cost. The other parameters, given in Table 3, are instead chosen based on the recommended values in the literature.

Table 3
The tuning parameters in the optimization program.

Tuning parameters	Value
Population size	300
Maximum number of generation	200
Probability of crossover	90%
Probability of mutation	1%
Selection process	Tournament
Tournament size	2

5.4. Selection of the final optimum design point

In multi-objective optimization, all of the obtained points from the Pareto front can be chosen as the optimal design point of the plant. However, in most of the cases, one final point should be selected based on the importance of each objective for the decision maker. In the present work, the criterion which has been taken into consideration to select the final optimal design point amongst the Pareto front's solutions is the primary energy saving (PES) index calculated based on the electrical and thermal efficiency of each point. The primary energy saving (PES) index is determined according to the EU Directive (Directive, 2004) on cogeneration (Conde Lázaro et al., 2006):

$$PES = 1 - 1 \Big/ \left[\frac{\eta_{net,el}}{\eta_{el,cogen} \times p} + \frac{\eta_{th}}{\eta_{th,cogen}} \right] \quad (25)$$

where the reference electrical and thermal efficiency for the separate generation of electricity and heat are 52.5% and 90% and the intermediate grid efficiency coefficient, p, is equal to 0.8925.

6. Results and discussion

6.1. Reformer and HT-PEM stack model validation

Considering the same geometrics and kinetic characteristics of the real plant during the simulation, the obtained results from the steam methane reformer and water gas shift reactor model have been compared with the experimental ones taken from an LT-PEM fuel cell based CHP plant (Sidera30), designed by ICI Caldaie S. p.A. At the same operating conditions, the syngas composition at the outlet of the reformer and the WGS reactor as well as the temperatures of the syngas leaving the fuel processor and the superheater from the model and experimental data were analyzed. The details regarding the validation procedure and accuracy of the developed model have been represented in the previous work of the authors (Najafi et al., 2015a).

The experimentally validated model developed by Bergmann et al (Bergmann et al., 2010). has been used to verify the accuracy of the HT-PEM model in this study. In this regard, the polarization curves of the fuel cell obtained from model and the one reported by Bergmann et al (Bergmann et al., 2010). at different CO concentrations have been compared. The details of the validation process and the obtained results from the fuel cell model can be found in the previous work of the authors (Najafi et al., 2015a).

6.2. Full load operation optimization

6.2.1. Optimization procedure I: considering thermal and electrical outputs as objectives

The Pareto front curve obtained from the multi-objective optimization of the plant, with net electrical generation and thermal generation as objectives, is illustrated in Fig. 4. It can be observed that an attempt to increase the thermal power output leads to a reduction in the net electrical generation of the plant. Achieving thermal generation up to 59 kW mildly deteriorates the electrical output while any further rise in the thermal generation leads to drastic loss of the electrical output. As is showed in Fig. 4, the Pareto front curve displays two ultimate points (points A and B) where the optimization can be seen as a single objective optimization. Point A

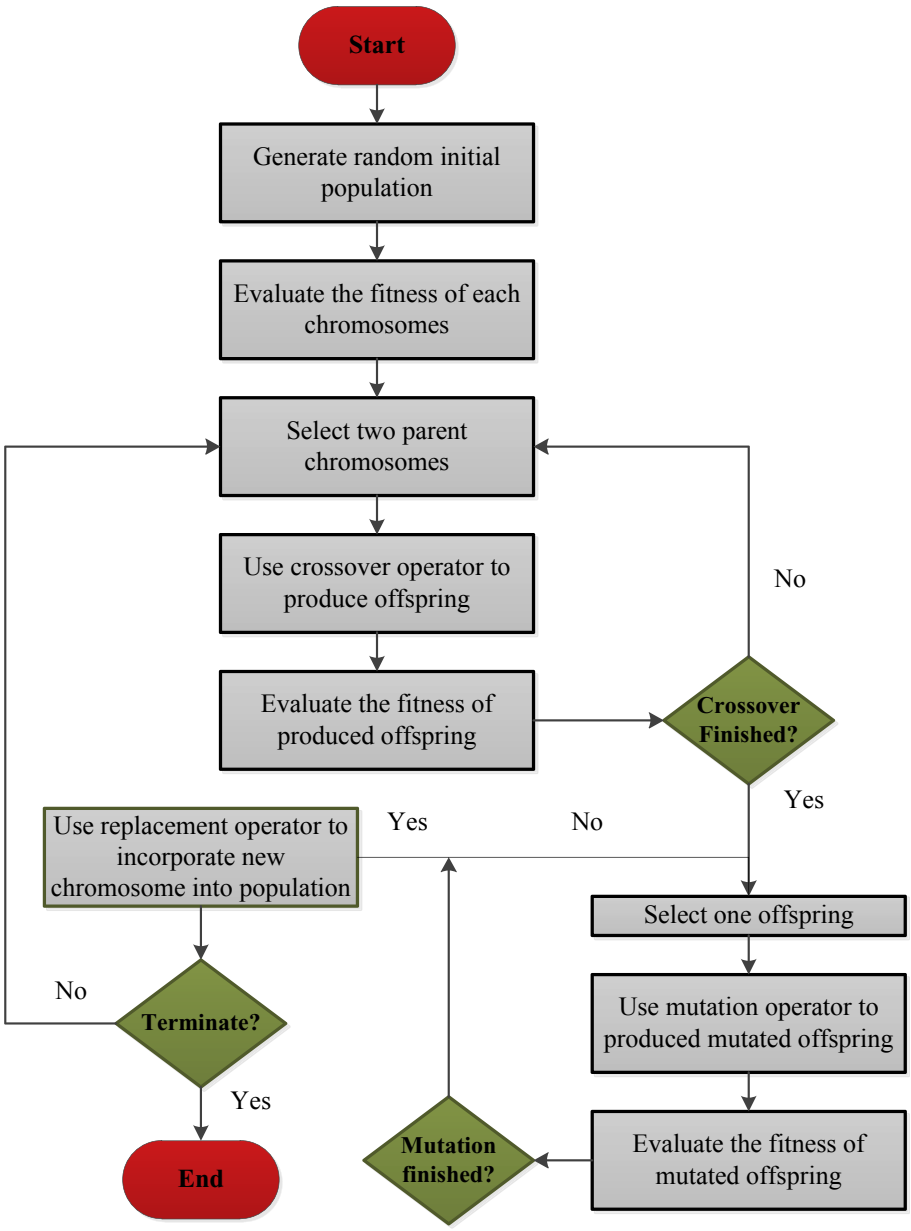

Fig. 3. Flowchart of genetic algorithm technique for plant optimization.

represents the situation in which the net electrical efficiency is most weighted, while point B is mostly weighted in favor of thermal efficiency. The maximum net electrical output can be reached at design point A (29.44 kW), while point B offers the highest value of thermal output of 63.29 kW. The values of design parameters and the corresponding performance-related results of points A and B are listed in Table 4. Capability of answering a wide range of electrical and thermal demand is one of the most crucial characteristics of a CHP system, which can broaden its applications and greatly influence its acceptance by the market. As can be seen in Fig. 4, a wide range of electrical generation starting from 21.0 kW to 29.4 kW and thermal generation from 54.0 kW to 63.3 kW can be supplied by the plant while, thanks to the multi-objective optimization, at each specific electrical (thermal) output, Pareto front offers the highest possible thermal (electrical) generation. As can be noticed by comparing the reported results for the two extreme cases in Table 4, aiming at optimizing of the electrical generation (i.e. point A), higher value of S/C and lower value of anodic stoichiometric ratio have been obtained. Smaller value of anodic stoichiometric ratio for point A can be justified considering the fact that lowering the value of λ_{H_2} increases the hydrogen utilization within the fuel cell which, subsequently, improves the electrical generation. In contrast, at higher values of anodic stoichiometric ratio, the amount of unreacted hydrogen in the stream leaving the anodic side of the fuel cell, which is later injected into the burner, increases. Accordingly, the available thermal energy to high pressure and low pressure water circuits in the superheater and the economizer augments which means higher thermal power generation (point B). In order to elucidate the impact of variation in steam to carbon ratio on the electrical and thermal generation, two counteractive phenomena should be taken into account. First, an increment in S/C causes higher reaction rate within the steam reformer, which eventually leads to higher hydrogen production available for electrochemical reactions. However, this gain is

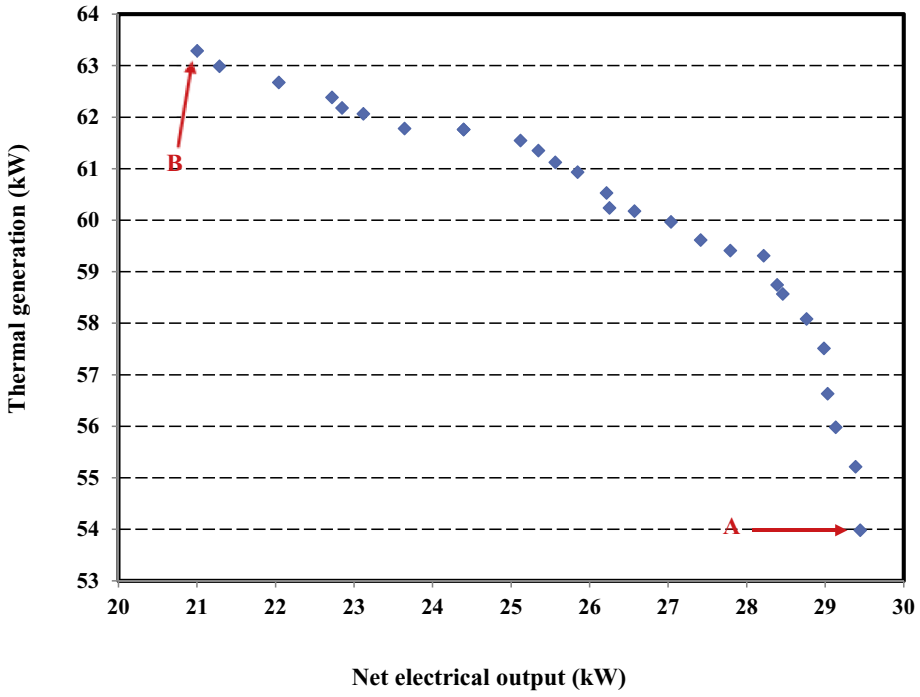

Fig. 4. Pareto front obtained from multi-objective optimization procedure I.

Table 4
Design parameters and performance indices of the system at points A and B for optimization procedure I.

Parameter	Electrical power optimization (point A)	Thermal power optimization (point B)
S/C	5.09	4.00
λ_{H2}	1.20	1.99
T_B	1217.2	1177.9
Aux/Proc	0.220	0.218
η_{ele} (%)	30.20	20.47
η_{th} (%)	55.37	61.70
PES	20.62	10.91
P_{ele} (kW)	29.44	21.00
P_{th} (kW)	53.98	63.29

attenuated by the lower rate of reforming reactions due to the lower temperature of the superheated steam entering the ejector at high S/C values (i.e. high water flow rate). In the case of point A, in order to lessen the adverse effect of high S/C, higher values of burner outlet temperature and auxiliary to process ratio have been selected by the GA to maximize the electrical power generation.

As mentioned earlier in Section 5.4, PES can be considered as a way to incorporate the performance of the system in terms of electrical and thermal efficiency into a single value. In this regard, the values of PES calculated based on the thermal and electrical efficiency of points A and B are represented in Table 4. As can be noticed in the table, the PES value for point A is almost twice that of point B; the fact which is due to the high electrical efficiency of the system at the operating conditions of point A.

6.2.2. Optimization procedure II: considering efficiencies as objectives

Fig. 5 depicts the Pareto optimal solutions achieved from the multi-objective optimization of the CHP plant, considering the net electrical efficiency and the thermal efficiency as objective functions. Analogous to the conflicting relation between the electrical and thermal generation, there is a contradictory relation between the two objectives and as one improves, the other objective deteriorates. Increasing the electrical efficiency from 20% to 23% does not affect the thermal efficiency greatly; however, further increment in the electrical efficiency results in a sharp fall in the thermal efficiency. Two extreme cases (point A and point B) can be considered in Fig. 5, where in each case, maximization of one of the objective functions is the ultimate goal. Taking into account the highest achievable electrical efficiency, point A leads to the net electrical efficiency of 29.54%, though operating at this point brings about the least thermal efficiency. In contrast, the design point B is the most desirable operating point in terms of thermal efficiency (leading to thermal efficiency of 61.13%), but it results in the lowest net electrical efficiency.

Comparing the values of design parameters corresponding to the Pareto front solutions, shown in Table 5, it can be concluded that in the regions with higher thermal efficiency and lower electrical efficiency, anodic stoichiometric ratio and aux/process ratio have values close to the maximum in their domains. As mentioned in the previous section, increasing the anodic stoichiometric ratio decreases the amount of hydrogen utilization in the stack and, in turn, deteriorates the electrical efficiency. In spite of this negative effect on electrical efficiency, employing higher anodic stoichiometric ratios increases the heat gain in the economizer and improves the thermal efficiency. Regarding the influence of aux/proc fuel ratio, increasing this parameter leads to higher amount of available heat within the methane reformer and consequently higher rates of reforming reactions and electrical power output from the stack. One should keep in mind that an increment in aux/proc fuel ratio directly augments the total chemical energy input to the plant (denominator of the net electrical efficiency equation (Eq. (14))) which offsets the aforementioned improvement in the net electrical output of the system and leads to lower electrical efficiencies. The variations of design parameters for the solutions given by the Pareto front (Fig. 5) are presented in Fig. 6. Considering the distribution of the design parameters in their allowable domains,

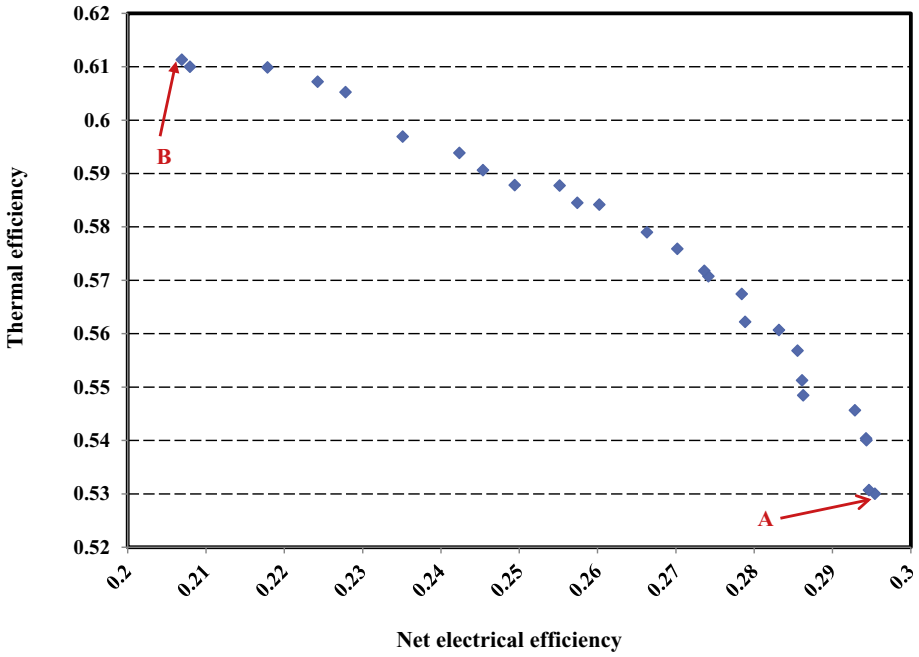

Fig. 5. Pareto front obtained from multi-objective optimization procedure II.

Table 5
The values of system design parameters of optimal points chosen considering three different criteria.

Fuel partialization	Optimization Objective	S/C	λ_{H2}	T_B	Aux/Proc
Full load (Procedure II)	Max PES	4.25	1.22	1233.7	0.131
	Max η_{ele}	4.64	1.21	1235.8	0.129
	Max η_{th}	4.03	1.99	1194.0	0.218
90%	Max PES	4.18	1.24	1240.1	0.166
	Max η_{ele}	4.35	1.20	1251.7	0.121
	Max η_{th}	4.10	1.81	1213.5	0.207
80%	Max PES	4.12	1.22	1238.1	0.156
	Max η_{ele}	4.61	1.20	1262.8	0.124
	Max η_{th}	4.09	1.90	1219.3	0.197
70%	Max PES	4.15	1.22	1247.5	0.205
	Max η_{ele}	4.69	1.21	1256.3	0.128
	Max η_{th}	4.03	1.78	1179.0	0.216
60%	Max PES	4.11	1.20	1254.1	0.203
	Max η_{ele}	4.33	1.21	1263.1	0.129
	Max η_{th}	4.00	1.82	1223.7	0.218

anodic stoichiometric ratio and aux/proc fuel ratio have the widest distributions. This indicates that anodic stoichiometric ratio and aux/proc ratio play an important role in the trade-off between the net electrical and thermal efficiency. The anodic stoichiometric ratio can be considered as an effective tool to adjust the electrical and thermal generation according to the load profile and/or customer's demand. On the other hand, steam to carbon ratio and burner outlet temperature are concentrated in a narrow range of optimum values, which implies that they slightly contribute to the opposing relation between the two defined objectives.

6.3. *Partial load operation optimization*

In the partial load operation, the mass flow rate of the fuel fed to the plant is gradually decreased down to 60% of its initial value and the performance of the system at different fuel partialization levels has been monitored. Similar opposing relation between the electrical and thermal efficiency in the pareto front curve, as in the case of full load operation, can be seen in the partial load operation, as depicted in Fig. 7. Since the fuel flow rate is changed in each optimization curve (because of partialization) while the same fuel processor and fuel cell geometries are employed, the performance indices are expected to vary correspondingly. As demonstrated in Fig. 7, fuel partialization results in a downward and rightward shift of the Pareto front curve to the regions with higher electrical efficiency and lower thermal efficiency. The growth in the net electrical efficiency can be explained by taking into account the improvement in the reforming reactions within the steam reformer and the diminution in voltage losses within the stack owing to the partialization. At partial load operation, less hydrogen enters the stack and to have the same anodic stoichiometric ratio, the current imposed to the stack should be decreased, which brings about a reduction in the current density. Operation at lower current densities, as can be inferred from the cell's polarization curve, causes lower voltage losses and enhances the cell voltage and electrical efficiency. In order to justify the descending trend of thermal efficiency with fuel partialization, one should consider the effect of partialization on waste heat produced within the stack. Owing to the partialization, as explained before, the current density decreases which in turn leads to a considerable reduction in the

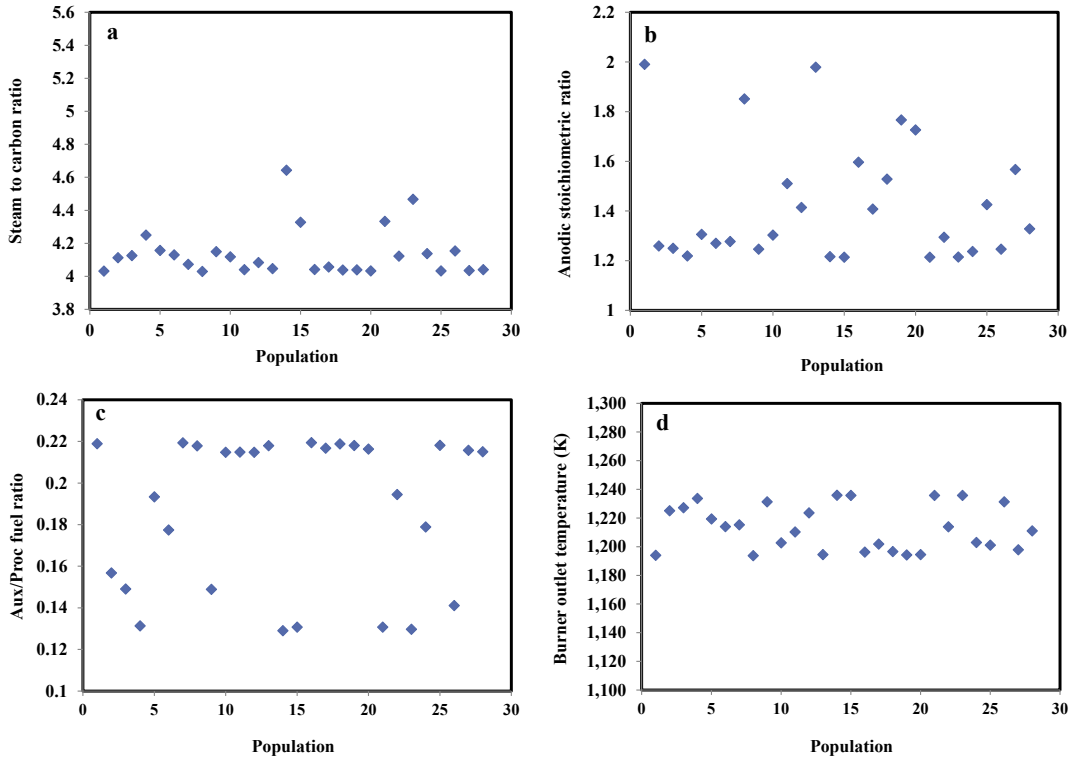

Fig. 6. Distribution of optimum values of design parameters for optimization procedure II.

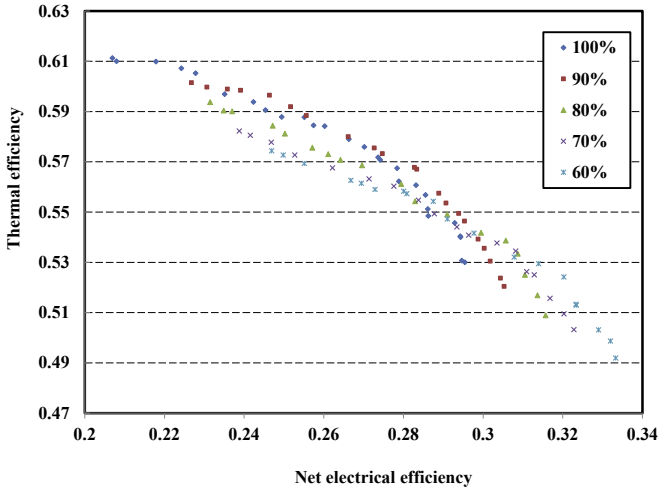

Fig. 7. Pareto front from multi-objective optimization of the plant at different fuel partialization levels.

voltage losses and the generated heat in the fuel cell per specific amount of provided fuel. It is noteworthy that exploiting the partialization strategy leads to a wide range of electrical and thermal efficiency of 20.7%–33.3% and 49%–61%.

In order to find the final optimum point based on the primary energy saving for each Pareto front curve at different fuel partialization levels, for each point presented in Fig. 7, PES value is calculated and the point with the highest value of PES has been considered as the most efficient operation point for the plant at each partialization level. The design parameters of the two ultimate points (highest net electrical efficiency and highest thermal efficiency) and the best design point based on PES at different levels of partialization are represented in Table 5. Additionally, the performance-related results of the CHP plant at the two extreme cases and the point selected based on the PES value are reported in Table 6. As the fuel partialization proceeds, due to the considerable improvement in the electrical efficiency, PES continues to augment, which means more efficient operation of the combined heat and power system. In the previous work of the authors (Najafi et al., 2015b), the values of net electrical efficiency at design operating conditions and different partialization levels have been reported. By comparing these results with the corresponding values for the highest net electrical efficiency from optimization (Table 6), up to 1% growth can be seen which could emphasize the importance of the optimization procedure.> Properties of the main nodes of the system, while operating at the optimal point which leads to the maximum electrical efficiency under full load operation, is demonstrated in Table 7. Similarly, Table 8 includes properties of the main nodes, while operating at the optimal point with the maximum electrical efficiency under 60% partial load.

7. Conclusion

In the present work, a multi-objective optimization procedure has been performed on an HT-PEM fuel cell based micro cogeneration plant to find the optimal solutions while considering the electrical and thermal efficiency as the objectives. The system consists of an HT-PEM fuel cell, methane reformer, water gas shift reactor and balance of plant. The multi-objective optimization has been conducted employing MATLAB optimization toolbox using genetic algorithm (GA) method. Anodic stoichiometric ratio, steam to carbon ratio, burner outlet temperature, and aux/proc fuel ratio have been chosen as design parameters. The Pareto front curves have been obtained for full load operation and operation at different levels of fuel partialization to locate the optimal operating conditions that can answer specific thermal and electrical load

Table 6
The performance indices of optimal points chosen considering three different criteria.

Fuel partialization	Optimization Objective	η_{ele} (%)	η_{th} (%)	PES	P_{ele}(kW)	P_{th} (kW)
Full load (Procedure II)	Max PES	29.28	54.56	18.79	27.87	51.93
	Max η_{ele}	29.54	53.0	17.98	28.05	50.23
	Max η_{th}	20.69	61.13	10.78	21.21	62.67
90%	Max PES	29.39	54.95	19.21	25.95	48.52
	Max η_{ele}	30.53	52.05	18.69	25.91	44.17
	Max η_{th}	22.68	60.15	13.22	21.28	56.90
80%	Max PES	30.86	53.35	20.09	23.87	41.84
	Max η_{ele}	31.57	50.89	19.29	23.74	38.31
	Max η_{th}	23.15	59.37	13.32	18.65	48.01
70%	Max PES	30.81	53.45	20.09	21.85	37.91
	Max η_{ele}	32.28	50.32	19.88	22.18	34.91
	Max η_{th}	23.88	58.22	13.54	17.09	42.18
60%	Max PES	32.02	52.42	21.01	19.45	31.85
	Max η_{ele}	33.33	49.19	20.50	18.99	28.04
	Max η_{th}	24.69	57.44	14.17	15.18	35.94

Table 7
Properties of the main nodes of the CHP system with the maximum electrical efficiency under full load operation (S/C = 4.64, aux/proc = 0.129, T_B = 963 °C, and λ_{H_2} = 1.21).

Node	Temperature (°C)	Flow rate (mol/s)	Composition (mole fraction)						
			H_2O	CH_4	H_2	CO	CO_2	N_2	O_2
5	434	0.601	82.30	17.40	0.00	0.00	0.00	0.30	0.00
6	963	1.431	13.24	0.00	0.00	0.22	8.04	67.72	10.77
7	577	0.762	46.09	3.20	39.93	2.30	8.25	0.22	0.00
8	320	0.762	46.09	3.20	39.93	2.30	8.25	0.22	0.00
9	342	0.762	44.21	3.20	41.81	0.42	10.13	0.22	0.00
13	179	0.516	17.62	4.73	61.74	0.62	14.96	0.33	0.00
14	161	0.218	26.93	11.19	25.00	1.47	35.41	0.00	0.00
15	605	1.431	13.24	0.00	0.00	0.22	8.04	67.72	10.77
34	90	1.260	0.00	0.00	0.00	0.00	0.00	79.10	20.90
35	161	1.424	20.83	0.00	0.00	0.00	0.00	69.97	9.20

Table 8
Properties of the main nodes of the CHP system with the maximum electrical efficiency under 60% partial load (S/C = 4.33, aux/proc = 0.129, T_B = 990 °C, and λ_{H_2} = 1.21).

Node	Temperature (°C)	Flow rate (mol/s)	Composition (mole fraction)						
			H_2O	CH_4	H_2	CO	CO_2	N_2	O_2
5	438	0.341	81.25	18.46	0.00	0.00	0.00	0.29	0.00
6	990	0.793	12.59	0.00	0.00	0.33	8.70	67.81	10.57
7	589	0.440	43.23	3.02	42.25	2.84	8.43	0.23	0.00
8	324	0.440	43.23	3.02	42.25	2.84	8.43	0.23	0.00
9	350	0.440	40.95	3.02	44.52	0.57	10.70	0.23	0.00
13	184	0.282	7.81	4.72	69.52	0.89	16.71	0.35	0.00
14	160	0.121	19.50	10.87	27.97	2.16	39.50	0.00	0.00
15	604	0.793	12.59	0.00	0.00	0.33	8.70	67.81	10.57
34	90	0.775	0.00	0.00	0.00	0.00	0.00	79.10	20.90
35	160	0.855	18.87	0.00	0.00	0.00	0.00	71.69	9.44

profiles. By optimizing the system at full load condition, while considering the electrical efficiency as the only objective, the net electrical efficiency of 29.5% was obtained. The optimal net electrical efficiency of 33.3% was also obtained at 60% partial load; which is 1% more than the efficiency that could be obtained using normal operation conditions. Optimizing the system at different partialization level resulted in optimal points with a wide range of electrical (20.7%–33.3%) and thermal efficiencies (49%–61%). Based on the primary energy saving index, the best operating points, in terms of electrical and thermal efficiency, have been found for the full load and each partial load operation. PES value increases steadily with fuel partialization starting from 18.8% at full load operation to 21% at 60% fuel partialization. The ultimate aim of this study was enabling the user to run the system at the best operating conditions at which the plant works in the most efficient way in terms of electrical and thermal efficiency while catering a specific thermal and electrical load.

Acknowledgment

This work was carried out in the framework of the project Microgen30 (EE01_00013) funded by Italian Ministry of Economic Development with the program Industria2015. The authors would also like to acknowledge ICI Caldaie S.p.A for providing technical support for this project.

References

Arsalis, A., Kær, S.K., Nielsen, M.P., 2015. Modeling and optimization of a heat-pump-assisted high temperature proton exchange membrane fuel cell micro-combined-heat-and-power system for residential applications. Appl. Energy 147, 569–581.

Arsalis, A., Nielsen, M.P., Kær, S.K., 2013. Optimization of a high temperature PEMFC

micro-CHP system by formulation and application of a process integration methodology. Fuel Cells 13, 238–248.
Baschuk, J.J., Li, X., 2003. Modelling CO poisoning and O2 bleeding in a PEM fuel cell anode. Int. J. Energy Res. 27, 1095–1116.
Basu, S., 2015. Proton exchange membrane fuel cell technology: India's perspective. Proc. Indian Natl. Sci. Acad. 81, 865–890.
Bazmi, A.A., Zahedi, G., Hashim, H., 2015. Design of decentralized biopower generation and distribution system for developing countries. J. Clean. Prod. 86, 209–220.
Benveniste, G., Pucciarelli, M., Torrell, M., Kendall, M., Tarancón, A., 2017. Life Cycle
Assessment of microtubular solid oxide fuel cell based auxiliary power unit systems for recreational vehicles. J. Clean. Prod. 165, 312–322.
Bergmann, A., Gerteisen, D., Kurz, T., 2010. Modelling of CO poisoning and its dynamics in HTPEM fuel cells. Fuel Cells 10, 278–287.
Besagni, G., Mereu, R., Chiesa, P., Inzoli, F., 2015. An Integrated Lumped Parameter-CFD approach for off-design ejector performance evaluation. Energy Convers. Manag. 105, 697–715.
Besagni, G., Mereu, R., Inzoli, F., Chiesa, P., 2017. Application of an integrated lumped
parameter-CFD approach to evaluate the ejector-driven anode recirculation in a PEM fuel cell system. Appl. Therm. Eng. 121, 628–651.
Cappa, F., Facci, A.L., Ubertini, S., 2015. Proton exchange membrane fuel cell for cooperating households: a convenient combined heat and power solution for residential applications. Energy 90, 1229–1238.
Chatrattanawet, N., Hakhen, T., Kheawhom, S., Arpornwichanop, A., 2017. Control
structure design and robust model predictive control for controlling a proton exchange membrane fuel cell. J. Clean. Prod. 148, 934–947.
Colella, W.G., Pilli, S.P., 2015. Energy system and thermoeconomic analysis of combined heat and power high temperature proton exchange membrane fuel cell systems for light commercial buildings. J. Fuel Cell Sci. Technol. 12.
Conde Lázaro, E., Ramos Millán, A., Reina Peral, P., 2006. Analysis of cogeneration in the present energy framework. Fuel Process. Technol. 87, 163–168.
Dillon, H.E., Colella, W.G., 2015. Independent analysis of real-time, measured per-formance data from microcogenerative fuel cell systems installed in buildings.
J. Fuel Cell Sci. Technol. 12.
Directive, E., 2004. Directive 2004/8/EC of the European parliament and of the council of 11 February 2004 on the promotion of cogeneration based on a useful heat demand in the internal energy market and amending Directive 92/42/EEC. Offic. J. Eur. Union 50–60.
Eames, I.W., Aphornratana, S., Haider, H., 1995. A theoretical and experimental study of a small-scale steam jet refrigerator. Int. J. Refrig. 18, 378–386.
Elmer, T., Worall, M., Wu, S., Riffat, S.B., 2015. Fuel cell technology for domestic built environment applications: state of-the-art review. Renew. Sustain. Energy Rev. 42, 913–931.
Evangelisti, S., Tagliaferri, C., Brett, D.J.L., Lettieri, P., 2017. Life cycle assessment of a polymer electrolyte membrane fuel cell system for passenger vehicles. J. Clean. Prod. 142, 4339–4355.
Fuchs, G., Hinderer, N., 2016. Towards a low carbon future: a phenomenology of local electricity experiments in Germany. J. Clean. Prod. 128, 97–104.
Gandiglio, M., Lanzini, A., Santarelli, M., Leone, P., 2014. Design and optimization of a proton exchange membrane fuel cell CHP system for residential use. Energy Build. 69, 381–393.
Godat, J., Marechal, F., 2003. Optimization of a fuel cell system using process integration techniques. J. Power Sources 118, 411–423.
Haghighat Mamaghani, A., Najafi, B., Casalegno, A., Rinaldi, F., 2017. Predictive
modelling and adaptive long-term performance optimization of an HT-PEM fuel cell based micro combined heat and power (CHP) plant. Appl. Energy 192, 519–529.
Haghighat Mamaghani, A., Najafi, B., Shirazi, A., Rinaldi, F., 2015. 4E analysis and multi-objective optimization of an integrated MCFC (molten carbonate fuel cell) and ORC (organic Rankine cycle) system. Energy 82, 650–663.
Ham, S.W., Jo, S.Y., Dong, H.W., Jeong, J.W., 2015. A simplified PEM fuel cell model for building cogeneration applications. Energy Build. 107, 213–225.
Hawkes, A.D., Brett, D.J.L., Brandon, N.P., 2009. Fuel cell micro-CHP techno-economics: Part 1–model concept and formulation. Int. J. Hydrogen Energy 34, 9545–9557.
He, Li, Wang, 2009. Progress of mathematical modeling on ejectors. Renew. Sustain. Energy Rev. 13, 1760–1780.
Herdem, M.S., Farhad, S., Hamdullahpur, F., 2015. Modeling and parametric study of a methanol reformate gas-fueled HT-PEMFC system for portable power generation applications. Energy Convers. Manag. 101, 19–29.
Hua, T., Ahluwalia, R., Eudy, L., Singer, G., Jermer, B., Asselin-Miller, N., Wessel, S., Patterson, T., Marcinkoski, J., 2014. Status of hydrogen fuel cell electric buses worldwide. J. Power Sources 269, 975–993.
Hubert, C.-E., Achard, P., Metkemeijer, R., 2006. Study of a small heat and power PEM fuel cell system generator. J. Power Sources 156, 64–70.
Kang, K., Yoo, H., Han, D., Jo, A., Lee, J., Ju, H., 2015. Modeling and simulations of fuel cell systems for combined heat and power generation. Int. J. Hydrogen Energy 41, 8286–8295.
Lau, L.C., Lee, K.T., Mohamed, A.R., 2012. Global warming mitigation and renewable
energy policy development from the Kyoto Protocol to the Copenhagen Accord -a comment. Renew. Sustain. Energy Rev. 16, 5280–5284.
Liu, F., Groll, E.A., 2013. Study of ejector efficiencies in refrigeration cycles. Appl. Therm. Eng. 52, 360–370.
Liu, Z., Wainright, J.S., Litt, M.H., Savinell, R.F., 2006. Study of the oxygen reduction
reaction (ORR) at Pt interfaced with phosphoric acid doped polybenzimidazole at elevated temperature and low relative humidity. Electrochim. Acta 51, 3914–3923.
Mehrpooya, M., Sayyad, S., Zonouz, M.J., 2017. Energy, exergy and sensitivity analyses of a hybrid combined cooling, heating and power (CCHP) plant with molten carbonate fuel cell (MCFC) and Stirling engine. J. Clean. Prod. 148, 283–294.
Merkel, E., McKenna, R., Fehrenbach, D., Fichtner, W., 2017. A model-based assess-ment of climate and energy targets for the German residential heat system. J. Clean. Prod. 142, 3151–3173.
Najafi, B., Haghighat Mamaghani, A., Baricci, A., Rinaldi, F., Casalegno, A., 2015a.
Mathematical modelling and parametric study on a 30 kWel high temperature PEM fuel cell based residential micro cogeneration plant. Int. J. Hydrogen En-ergy 40, 1569–1583.
Najafi, B., Mamaghani, A.H., Rinaldi, F., Casalegno, A., 2015b. Fuel partialization and power/heat shifting strategies applied to a 30 kW el high temperature PEM fuel cell based residential micro cogeneration plant. Int. J. Hydrogen Energy 40, 14224–14234.
Najafi, B., Najafi, H., Idalik, M., 2011. Computational fluid dynamics investigation and multi-objective optimization of an engine air-cooling system using genetic al-gorithm. Proc. Inst. Mech. Eng. Part C J. Mech. Eng. Sci. 225, 1389–1398.
Napoli, R., Gandiglio, M., Lanzini, A., Santarelli, M., 2015. Techno-economic analysis
of PEMFC and SOFC micro-CHP fuel cell systems for the residential sector. En-ergy Build. 103, 131–146.
Pirkandi, J., Ghassemi, M., Hamedi, M.H., Mohammadi, R., 2012. Electrochemical and thermodynamic modeling of a CHP system using tubular solid oxide fuel cell (SOFC-CHP). J. Clean. Prod. 29–30, 151–162.
Pirkandi, J., Mahmoodi, M., Ommian, M., 2017. An optimal configuration for a solid
oxide fuel cell-gas turbine (SOFC-GT) hybrid system based on thermo-economic modelling. J. Clean. Prod. 144, 375–386.
Pisani, L., 2008. Multi-component gas mixture diffusion through porous media: a 1D analytical solution. Int. J. Heat Mass Transf. 51, 650–660.
Rizzi, F., Annunziata, E., Liberati, G., Frey, M., 2014. Technological trajectories in the automotive industry: are hydrogen technologies still a possibility? J. Clean. Prod. 66, 328–336.
Sharaf, O.Z., Orhan, M.F., 2014. An overview of fuel cell technology: fundamentals and applications. Renew. Sustain. Energy Rev. 32, 810–853.
Siegel, C., Bandlamudi, G., Heinzel, A., 2011. Systematic characterization of a PBI/H3PO4 sol–gel membrane—Modeling and simulation. J. Power Sources 196, 2735–2749.
Stambouli, A.B., 2011. Fuel cells: the expectations for an environmental-friendly and sustainable source of energy. Renew. Sustain. Energy Rev. 15, 4507–4520.
Tran, T.T.D., Smith, A.D., 2017. Evaluation of renewable energy technologies and their potential for technical integration and cost-effective use within the U.S. energy sector. Renew. Sustain. Energy Rev. 80, 1372–1388.
Varga, S., Oliveira, A.C., Diaconu, B., 2009. Numerical assessment of steam ejector efficiencies using CFD. Int. J. Refrig. 32, 1203–1211.
Wang, J., 2017. System integration, durability and reliability of fuel cells: challenges and solutions. Appl. Energy 189, 460–479.
Wang, Y., Chen, K.S., Mishler, J., Cho, S.C., Adroher, X.C., 2011. A review of polymer electrolyte membrane fuel cells: technology, applications, and needs on fundamental research. Appl. Energy 88, 981–1007.
Wee, J.H., 2007. Applications of proton exchange membrane fuel cell systems. Renew. Sustain. Energy Rev. 11, 1720–1738.
Wee, J.H., 2010. Contribution of fuel cell systems to CO2 emission reduction in their application fields. Renew. Sustain. Energy Rev. 14, 735–744.
Xu, J., Froment, G.F., 1989. Methane steam reforming, methanation and water-gas shift: I. Intrinsic kinetics. AIChE J. 35, 88–96.
Zhai, Q., Cao, H., Zhao, X., Yuan, C., 2014. Assessing application potential of clean energy supply for greenhouse gas emission mitigation: a case study on General Motors global manufacturing. J. Clean. Prod. 75, 11–19.
Zheng, L., Deng, J., 2017. Research on CO2 ejector component efficiencies by
experiment measurement and distributed-parameter modeling. Energy Conv-ers. Manag. 142, 244–256.